NASA TECHNICAL MEMORANDUM

NASA TM X-62,264

NASA TM X-62,264

MARTIAN LINEAMENTS FROM MARINER 6 AND 7 PHOTOGRAPHS

Peter H. Schultz and F. Earl Ingerson

Ames Research Center
Moffett Field, Calif. 94035

and

Department of Geological Sciences
University of Texas at Austin
Austin, Texas 78712

April 1973

MARTIAN LINEAMENTS FROM MARINER 6 AND 7 PHOTOGRAPHS

Peter H. Schultz

Planetary Science and Applications Branch

NASA-Ames Research Center

Moffett Field, Calif. 94035

and

F. Earl Ingerson

Department of Geological Sciences

University of Texas at Austin

Austin, Texas 78712

ABSTRACT

Mariner 6 and 7 photographs were used to investigate the nature and importance of linear surface trends on Mars. Cross correlations of frequency-azimuth distributions of linear trends from different Mariner frames indicate that lineations not recognized as topographic features have a component of pseudoforms, probably introduced during digital reconstruction of the pictures. Similar statistical tests may aid in the analysis of surface trends from future satellites and space probes. In this study, the most reliable data were separated into photometrically defined provinces. Meridiani Sinus and Margaritifer Sinus display five major trends in common, which are interpreted as extensions of crustal weaknesses related to the enormous equatorial canyon revealed in Mariner 6 and 9 pictures. Alignments of crater wall segments generally match these trends and suggest structural control of crater plan. Crater chains, however, do not match these trends and are interpreted as secondary impacts. Rose diagrams of lineations in Deucalionis Regio exhibit much more complexity and are believed to reflect a better preserved or more complex geologic history.

MARTIAN LINEAMENTS FROM MARINER 6 AND 7 PHOTOGRAPHS

Introduction

Mariner 6 and 7 photographs suggest a complex structural history of the Martian surface that is expressed by numerous lineations of various topographic form. Binder and McCarthy (1972) proposed that such lineations on Mars comprise at least two systems, one of which is expressed on a global scale as postulated by Meinesz (1947), the other, associated with large basins. Strom (1964) made an extensive survey of the lunar grid system, and comparisons with Mars (Binder, 1966; Binder and McCarthy, 1972) may imply a common structural history of planetary bodies perhaps resulting from a decrease in their rotation or polar wandering. The separate study presented here considers the preferred orientations of the trends in the nonpolar regions included in the Mariner 6 and 7 wide-angle (A camera) photography. Regionally distinct structural histories are sought rather than a global system.

Approach

Enlargements were made at three contrast scales from maximum discriminability versions of the computer-processed data. The different contrasts provided a check for pseudoforms and residual noise in the processed photographs. Lineations were mapped directly on the unrectified photographs and were assigned one of three values corresponding to the observer's (P.H.S.) ability to recognize lineations as topographic features (Figure 1). The most significant class of lineations (w3) represents forms identified as positive or

negative relief through recognition of adjacent dark and light regions indicating changes in slope. The marginally significant class of lineations (w2) are identified as positive or negative relief but not with the same confidence as those in the w3 class. The least significant lineations (w1) are recognized clearly as linear features but cannot be distinguished as relief. The last lineation class might be confused with coherent noise (see Rindfleisch, et al., 1971) introduced during electronic imaging. Comparisons between the A-camera (wide-angle) and B-camera (telephoto) photographs confirmed the identification of several w1 lineations on A-camera photographs as true surface features. In a few examples, narrow lineations recognized in A-camera photographs were recognized in nested B-camera photographs, even though the lineations were narrower than a picture element (pixel) in the A-camera version. This may indicate a general albedo or spectral contrast associated with such lineations. The unrectified photographs (Figure 1) have greater information content than the rectified (orthographically projected) versions and consequently were used as guides for identification on the rectified photographs (Figure 2).

The detectability of lineations strongly depends on the local solar elevation, photographic scale, and obliqueness of view. The first two parameters were supplied by the Pegasis data (Campbell, 1970) and were mapped as contours for each unrectified photograph. We included the effects of the obliqueness of view by dividing the photographic scale (surface distance per picture element) by the cosine of the emission angle (angle between the camera's optical axis and surface normal). This correction strictly applies only for lineations

trending perpendicular to the optical axis of the imaging system. Empirical studies by Keene (1965) related solar elevation to visual identification of surface detail and provide relative values of detectability dependent on local solar elevation. For example, a surface feature barely recognized at a solar elevation of 14° must be four times as large for recognition at a solar elevation of 65°. Consequently, multiplication of these relative values by the adjusted photographic scale gives discernibility indices (Figure 1) that illustrate the relative change in the detection threshold of surface features having the same morphologic form. An index of 4 in Mariner 6 frame 6N07 means that a lineation trending perpendicular to the optical axis of the imaging system must be four times wider than a lineation in Mariner 6 frame 6N19 (an index of 1) in order to be recognized. These indices do not include the effects of atmospheric haze, which may be significant. Meaningful morphologic studies from photographic Mariner missions require an appreciation for changes in discernibility across a single frame as well as between different frames.

The azimuth and length of mapped lineations were measured for both unrectified and rectified photographs. Lineations that exhibited abrupt changes in plan were segmented and treated as distinct lineation trends. In unrectified photographs, an arbitrary "north" direction corresponded to the vertical edge of the picture format, whereas in rectified photographs, coordinate overlays from the Jet Propulsion Laboratory (Campbell, 1970) gave the local north direction. Frequency-azimuth distributions of the lineations for each

photograph and each lineation weight were compiled (Figure 3, a and b). Running means having a 4° window in azimuth smoothed the distributions in order to absorb human errors in azimuth measurements and to prepare the data for further statistical treatment.

Each lineation azimuth in the rectified photographs also was assigned one of three integral weights dependent on the lineation length. Lineations that are less than 21 km in length were assigned a weight of 1; between 21 km and 40 km, a weight of 2; and greater than 40 km, a weight of 3.

Autocorrelation and autopower functions were used for each frequency-azimuth distribution from each photograph as a monitor for possible constant intervals between dominant trends. In addition, these functions provided a qualitative check on the reliability of the data by comparisons with functions from randomly generated azimuths where there were relatively few lineations. The autocorrelation function for discrete data is given by:

$$C(\tau = m \cdot \Delta t) = \frac{\sum_{i=1}^{N-m} (x_i - \bar{x})\,(x_{i+m} - \bar{x})}{(N-m) \cdot \sigma_x^2} \qquad (1)$$

where τ is the lag, which is expressed in terms of equally spaced (Δt) data points for increasing intervals m = 0, 1, 2,...N; N represents the total number of data points; x_i and x_{i+m} are the functional values at points i and m, respectively; $\bar{x}$ is the mean value for all data points; and σ_x^2 is the sample variance. In this case, Δt is 1° of azimuth, N is 180°, and x_i and x_{i+m} are the number of lineations at azimuths i and i+m, respectively. Since the data in this case are azimuths, the series ends at N = 180°; however,

evaluation of the autocorrelation function only to this limit results in the elimination of possible correlations between lineations at 175° azimuth, for example, and 185° azimuth, which is simply 5°. Consequently, the autocorrelation function was modified to a "cyclic" autocorrelation function

$$C(\tau = m \cdot \Delta t) = \frac{\sum_{i=1}^{N} (x_i - \bar{x})(x_{i+m} - \bar{x})}{N \sigma_x^2} \qquad (2)$$

in which lineations between 0 and (i+m-180°) were repeated where (i+m) exceeded 180°. The autopower function is the fourier transform of the autocorrelation function. In this study, the Fast Fourier Transform (FFT) algorithm was used to calculate the autopower directly from the data rather than from the autocorrelation function (Webb, 1970). The resulting autopower corresponded to the autocorrelation discussed for equation (1) rather than equation (2).

The nonrandomness of these trends is confirmed both by comparison of randomly generated orientations and by comparison with the frequency of preferred trends from mapped lineations with a Poisson distribution. The significance of the trends with respect to their being actual surface features, however, can be tested by comparison of cross correlations between two unrectified photographs with cross correlations of corresponding rectified pairs. The cross correlation between functions x(t) and y(t) is defined in terms of the sample cross covariance,

$$R_{xy}(\tau) = \frac{1}{N} \sum_{t=0}^{(N-1)-|\tau|} \left[x(t) - \bar{x} \right] \left[y(t+|\tau|) - \bar{y} \right] \qquad (3)$$

where N is the total number of data points; $\bar{x}$ and $\bar{y}$ are the mean values of the functions x(t) and y(t), respectively; and τ is the displacement, or "lag", from the data point t. In this case, N is 180°; x(t) and y(t) are the number of lineations at azimuth t from two separate Mariner frames, x and y, and τ is the lag in degrees of azimuth. The cross correlation then is given by:

$$C_{xy}(\tau) = \frac{R_{xy}(\tau)}{\left[R_x(o) \cdot R_y(o)\right]^{\frac{1}{2}}} \qquad (4)$$

where $R_x(o)$ is the cross covariance at zero lag between x(t) and x(t), i.e., simply the auto covariance; similarly, $R_y(o)$ is auto covariance at zero lag for y(t).

If mapped lineations represent residual trends resulting from imaging, then a good cross correlation between frequency-azimuth distributions from unrectified photographic pairs should result regardless of the picture format. On the other hand, if the lineations are true surface trends, then a better cross correlation on rectified pictures might be expected if the surface trends are part of a generally well-defined system.

Straight wall segments of polygonal craters and crater chain alignments supplied additional data for linear surface trends. Each straight wall segment was weighted subjectively from 1 to 3 depending on the certainty of identification. Crater chains were divided into pairs of craters, and each pair was assigned a similar subjective weight from 1 to 3 according to their visibility. Straight wall segments, in general, are thought to be the results of slumping along structural weaknesses, whereas crater chains may be due to secondary ejecta or structurally controlled endogenic volcanism. Consequently, these two sets of

data were treated separately both with respect to each other and with respect to mapped lineations.

Photometrically corrected versions of the mapped regions showed the contacts between low-albedo and high-albedo provinces that have long been recognized through earth-based studies and recently compiled by de Vaucouleurs (1971). The data from rectified photographs were grouped into their respective photometric provinces so that possible tectonic provinces could be revealed.

Results

Figure 4 shows the frequency-azimuth distributions in polar coordinates (rose diagrams) for selected frames from Mariner 6. The most significant lineations (w3) were combined with the less significant lineations (w2) for a larger sample size (w3-w2). The lower half of each rose diagram corresponds to lineations weighted according to their apparent length, whereas the upper half represents unweighted lineations.

The rose diagrams of unrectified photographs show several features that result from electronic imaging and subsequent computer processing. The 'east-west' (horizontal) direction is typically devoid of lineations. This is not the result of east-west solar illumination, which commonly does not correspond to the 'east-west' direction of the picture format. It is more likely due to the removal of coherent noise parallel to the direction of tape transport as described by Rindfleisch, et al. (1971). The rectified photographs retain this gap in their rose diagrams. The arrows in the unrectified photographs (Figure 3a) indicate linear trends identified on unprocessed photographs. In

general, such trends were eliminated effectively during noise removal at JPL.

If the mapped lineations are true surface features, then they should be detected most easily where they are perpendicular to the direction of solar illumination. Such a selection effect in the rose diagrams generally exists for w3-w2 lineations but appears to be subordinate to either prominent east-west trending lineations or contamination of the data by pseudoforms for w1 lineations.

The rectified versions reveal several preferred trends. Frame 6N09 (Figure 3b) shows a prominent north-south lobe for both the w3-w2 and w1 lineations. Frame 6N13 (Figure 4a) displays a large N66E lobe, whereas 6N21 (Figure 4b) exhibits a preferred N34W orientation of lineations, which is almost perpendicular to that in 6N13.

After elimination of duplicate lineations in overlapping photographs, all of the w1 lineations (total number of 1506) from frames 6N07, 6N13, 6N17, 6N19, 6N21, and 6N23 were combined and revealed prominent trends near N25W, N05W, N50E, N63E, and N85E with less significant peaks near N30E and N40E (Figure 5a). Combination of 775 w3-w2 lineations from the same frames showed prominent trends near N25W, N05W, and N55E with less significant trends near N48W and N30E (Figure 5b). Consequently, four of the five trends in the w3-w2 lineations have corresponding trends in the w1 lineations, and this suggests that some of the w1 lineations are surface forms. For comparison, 259 straight wall segments from the same Mariner 6 frames exhibited prominent lobes near N50W, 25W, and N50E with less prominent peaks near N30E, N60E, and N70E (Figure 6a). All

but the less significant N60E and N70E trends have corresponding trends in the w3-w2 lineations. Crater chains (121 alignments) exhibited prominent narrow lobes at N53W and N62E (Figure 6b).

In general, cross correlations between distributions of w1 lineations from unrectified photographs exhibit relatively sharp peaks near zero lag, whereas the corresponding distributions from rectified photographs yield broader and smaller peaks that are offset from zero lag (Figure 7). The broadening and reduction of the cross-correlation peak are interpreted as effects of geometric stretching of the rectified photographs. The good cross correlation between unrectified pairs remained after the elimination (filtering) of data in the ranges N90W-N70W and N90E-N70E where typically few lineations occur in unrectified photographs. Inclusion of these voids in the frequency-azimuth distribution introduces an improved cross correlation that may be meaningless with respect to mapped trends.

Such statistical processing suggests that a significant component of pseudoforms dilute the least weighted set of lineations, despite the elimination of obvious noise patterns. This interpretation is supported by the correlation at zero lag between Mariner 6 and Mariner 7 unrectified photographs. In contrast, the frequency-azimuth distributions of the highest weighted lineations generally produced marginal improvements in the cross correlations of rectified pairs.

Cross correlations of 6N13-6N09 and 6N11-6N19 (w1 lineations), however, showed improvements in rectified pairs over the filtered unrectified pairs at zero lag. Although cross correlations of 6N07-6N13 and 6N13-6N11 did not

exhibit marked improvements in the rectified pairs, secondary peaks occurred at zero lag. These exceptions may reflect a regional dependence of preferred lineation trends since the above photographic pairs are in either the same or similar photometrically distinct provinces. Further discussion of this possibility is presented below. Such exceptions indicate that not all of the least weighted lineations are pseudoforms and therefore should not be eliminated completely from the final analysis.

Figure 8 shows the frequency-azimuth distribution of lineations in Meridiani Sinus, Margaritifer Sinus, which for this study includes Eos, and Deucalionis Regio, which for this study includes Aram. The less significant w1 lineations generally reflect the trends for the better defined w3-w2 lineations in Margaritifer Sinus and Meridiani Sinus. The prominent peaks of the two data sets from Deucaleonis Regio, however, do not match consistently. The most significant lineations from both Margaritifer Sinus (Figure 5c) and Meridiani Sinus (Figure 5d) display preferred trends within 3° of N40W, N16W, N08E, N33E, and N51E. Although the prominent N74E trend in Margaritifer Sinus is not matched exactly for w3-w2 lineations in Meridiani Sinus, it is matched by one of the most prominent trends of all data sets, which occurs for w1 lineations in Meridiani Sinus. In addition, a minor N69W trend from w3-w2 lineations in Margaritifer Sinus is close to the N67W trend from w3-w2 lineations in Meridiani Sinus. These relatively close matches of at least five out of six major trends in each province strongly suggest a similar structural history. Three preferred trends (N19W, N11E, and N29E) from w3-w2 lineations in Deucalionis Regio (Figure 5e) may correspond to several of the above trends, but they are among nine possibly significant peaks in the frequency-azimuth distribution.

Autocorrelation and autopower functions of the frequency-azimuth distributions from individual rectified frames generally reveal peaks at lags corresponding to 15°± 4° for w3-w2 lineations and to both 15°±5° and 28±2° for w1 lineations. Combinations of lineations into the three photometric provinces provide larger samples and, consequently, more reliable data for this type of analysis. These groupings also produce azimuthal harmonics at 15°±2° for w3-w2 lineations and at 15°±2° as well as 28°±2° for w1 lineations. Visual inspection of the frequency-azimuth distributions (Figure 5) confirms these intervals between trends. Such spacings suggest conjugate shear systems within the Martian crust.

The two most prominent trends of crater-wall segments (N30E and N72E) in Margaritifer Sinus (Figure 6c) approximately reflect the N33E and N72E trends recognized for w3-w2 lineations of Margaritifer Sinus and Meridiani Sinus (Figure 5c and d, respectively). In Meridiani Sinus (Figure 6d), the three most prominent crater-wall trends (N25W, N23E, and N61E) also correspond to the lineation trends in that province (Figure 5d) if a systematic 6° clockwise displacement in azimuth is allowed. Crater-wall trends in Deucalionis Regio (Figure 6e) exhibit eight possibly significant orientations, of which the three most prominent trends are at N48W, N31E, and N48E. The last two trends correspond to lineation trends in the other two provinces but are expressed poorly in the lineation trends in Deucalionis Regio (Figure 5e).

In contrast to crater-wall segments, the trends of crater chains separated into photometric provinces generally do not reflect consistently trends from w3-w2 lineations. Both Margaritifer Sinus and Meridiani Sinus display a

prominent crater-chain trend near N56W, which may be associated with the large basin Hellas. Margaritifer Sinus also includes two possibly related trends near N48E and N60E, both of which are absent in Meridiani Sinus. Deucalionis Regio exhibits a prominent trend at N61E but lacks the trend at N56W found in the other two provinces.

The region northeast of Hellas (frame 7N23) includes prominent N50E, N37E, and N21E trends (w3-w2 lineations) with a relatively minor N70W trend. Closer to the eastern rim of Hellas (frame 7N25), however, N00E and N15E trends are dominant. The N37E trend in frame 7N23 and the N15E trend in frame 7N25 are approximately concentric with the Hellas basin at their respective distances and orientations from the rim. Radially directed lineations from Hellas only occur in the w2 and w1 lineations and are subordinate to the concentric system. The dominance of the concentric system of lineations is similar to old lunar basins, such as Humorum and Nectaris, where the concentric structural weaknesses persist or are rejuvenated, whereas radial ejecta patterns are destroyed with age.

Discussion

Lineations are identified as a variety of topographic forms. Positive-relief lineations include ridges analogous to lunar wrinkle ridges, ejecta, scarps, and remnants of craters. Negative-relief lineations include grabenlike nonsinuous rilles, rectilinear rilles, curvilinear rilles, and coalesced craters. Several crater rim areas exhibit curvilinear rilles that converge toward a common area from the rim crest. These are suggested to represent

drainage features rather than ejecta or structurally produced rilles. The existence of such rilles is confirmed from Mariner 9 photographs (see M9-4219-51).

Clearly, the structural significance of preferred trends of lineations requires the elimination of both electronic imaging noise and nonstructurally produced forms, such as crater ejecta, topographically controlled drainage features, lineations on crater floors, and wind-produced forms. In addition, nonlinear features can be misinterpreted as lineations owing to poor resolution and the effects of solar illumination.

Removal of possibly nonstructural lineations from the highest weighted set did not alter significantly the trends described above. Deucalionis Regio displayed the greatest number of such lineations possibly as a result of the greater detectability of features in this region than that in Margaritifer Sinus and Meridiani Sinus. In particular, frames 6N17, 6N19, 6N21, and 6N23, which include Deucalionis Regio, have respective discernibility indices of 5.0 to 1.0, 2.0 to 1.1, 1.0, and 1.0. In contrast, frame 6N07 (Margaritifer Sinus) has discernibility indices ranging from 17 to 4, whereas frame 6N13 (Meridiani Sinus) has indices from 3.2 to 1.6. Consequently, the identification of specific morphologic form from Mariner 6 photographs, beyond positive or negative relief, should be more difficult in Margaritifer Sinus and Meridiani Sinus. The greater detectability in Deucalionis Regio, however, may not be offset by the ability to recognize the distinction between topographically controlled drainage features and structurally controlled features. Consequently, the complex rose diagram for this region may reflect the increased

detail recognized, a distinctive geologic history, or a combination of these two possibilities.

Several features support the interpretation that Deucalionis Regio and Aram have different geologic histories from Margaritifer Sinus and Meridiani Sinus. Prominent rectilinear and curvilinear rilles accompany the contacts between Aram and Margaritifer Sinus (Figure 2) as well as Deucalionis Regio and Meridiani Sinus (Figure 9). Although the rose diagram for Deucalionis Regio and Aram is complex, the preferred lineation trends in Margaritifer Sinus are generally similar to those in Meridiani Sinus; therefore, the latter two regions perhaps had similar structural histories. The domelike relief of Meridiani Sinus also may indicate locally contrasting tectonic development (Binder and McCarthy, 1972).

Deucalionis Regio exhibits a cratered terrain that morphologically resembles portions of the lunar surface. Frame 6N20 clearly reveals wrinkle-ridgelike features as well as a 13 km diameter crater with a concentric plan, which appears analogous to numerous lunar craters along the margins of maria. Such craters are interpreted as the result of volcanic modification of crater floors (Schultz, 1972). Frame 6N19 includes several flat-floored craters with breached walls. The surrounding crater density does not appear great enough to degrade significantly such large craters, and the breached walls resemble lunar craters inundated during the epochs of mare emplacement. Consequently, Deucalionis Regio may be a region that has been modified significantly by an epoch (or epochs) of endogenic activity such as volcanically produced flooding of crater floors. Detailed morphologic comparison of Deucalionis Regio to

other provinces is unwarranted owing to the large differences in discernibility indices from Mariner 6 and 7 photography. The preservation of its cratering history, and possibly its multistage endogenic modification, may account partially for the complex frequency-azimuth distribution of lineations.

The enormous canyon that corresponds to the photometrically lighter Eos appears to indicate relatively recent and large-scale tectonic events (Sharp, et al., 1971). The full extent of this feature has been revealed in the more recent Maringer 9 photographs (see McCauley, et al., 1972). The regional trends (w3-w2 lineations) in Meridiani Sinus generally correspond to trends in Margaritifer Sinus and Eos. Consequently, structural events related to the formation of the Eos canyon may extend farther to the east.

As the good cross correlations of unrectified photographs suggest, the general mismatch of preferred trends from w1 lineations and w3-w2 lineations may reflect dilution of the w1 lineations by pseudoforms. Published Mariner 9 photographs (Sagan, et al., 1972), however, show dark and light lineations that apparently are wind produced. Thus, it is suggested that some of the large peaks in the rose diagram of w1 lineations may reflect meteorologically controlled trends that will be distinct from w3-w2 lineations, which are identified as topographic forms. Preliminary examination of Mariner 9 photographs of this region confirms such a possibility.

As Binder and McCarthy (1972) point out, surface trends may correspond to ejecta and structural features associated with huge basins. If such basins are not included in the photographic coverage, it is difficult, if not impossible, to separate associated trends from regional or global structural

trends. This problem is particularly severe for photographic flyby missions such as the Mariner '69 and future space probes.

Conclusions

Mariner 6 and 7 photographs provided an intriguing glimpse into the structural complexity of the Martian crust that now has been confirmed by the highly successful Mariner 9 Orbiter. Experience with photographs from precursory probes indicates that caution must be used in mapping lineations. Cross correlations of lineations from separate frames having different orientations provide an index for the possible dilution of structural detail by imaging noise. Lineations that are not recognized as topographic relief are most likely to be confused with pseudoforms, but such lineations commonly represent the only data available in sufficient quantity for statistical treatment. Realization of and proper allowance for this problem are prerequisites for any study of planetary lineation systems from terrestrial satellites, such as ERTS-1, and space probes, such as the 1973 Mariner-Venus/Mercury, that have digital imaging systems.

Combinations of data from Mariner 6 according to regions defined by photometric boundaries reveal similar orientations of lineations at approximately 14° and 28° spacings for Meridiani Sinus and Margaritifer Sinus (plus Eos). This system probably represents conjugate shear fractures that are related to the formation of the canyon in Eos. Such a conclusion is consistent with an independent study of crustal fractures identified in the chaotic terrain from Mariner 6 frames 6N06, 07, 08, and 014, which include the Margaritifer

Sinus and Eos areas (Wilson et al., 1973). Deucalionis Regio (plus Aram) displays a more complex distribution of lineation trends that reflect a more complex or better preserved geologic history. The regions included in Mariner 6 photographs commonly are bordered by numerous rillelike lineations. Consequently, it is suggested that such boundaries in the restricted areas of this study may have physiographic and perhaps tectonic, as well as photometric, importance.

Inspections of Mariner 9 photographs showing the regions used in this study confirm the reliability of these data. The potentially higher resolution provided by Mariner 9 commonly is offset by the higher solar illumination (local solar zenith distance around 45°) so that the effective discernibility of linear features is comparable to Mariner 6 frame 6N21 (local solar zenith distance around 70°).

Acknowledgments

We are indebted to the labors of Robert Adams and Walker D. Manley, Jr., who aided in the measurements and reduction of data. In addition, Mr. Adams performed the initial computer programming. Carol Webb graciously supplied autopower and cross-power spectra subroutines, as well as advice, that were used in this analysis (see Webb, 1970). We also would like to thank William R. Muehlberger, Ron Greeley, and Verne Oberbeck for their review and constructive comments.

This research is funded by the Planetology Program Office, Office of Space Science, NASA Headquarters, under Grant NGR-44-012-194.

REFERENCES

Binder, A. B., Mariner IV: analysis of preliminary photographs, Science, 152, 1053, 1966.

Binder, A. B. and D. W. McCarthy, Jr., Mars: the lineament systems: Science, 176, 279, 1972.

Campbell, J. K., Mariner Mars 1969 simulated TV pictures (final), Jet Propul. Lab. 605-237, Cal. Inst. Tech., 1970.

Keene, G. C., Lunar Orbiter photo study Z-3841, Rochester, N. Y., Eastman Kodak Co., 137, 1965.

McCauley, J., M. H. Carr, J. A. Cutts, W. K. Hartmann, H. Masursky, D. J. Milton, R. P. Sharp, and D. E. Wilhelms, Preliminary Mariner 9 report on the geology of Mars, Icarus, 17, 289, 1972.

Meinesz, F. A. V., Shear patterns of the Earth's crust, Amer. Geophys. Union Trans., 28, 1, 1947.

Rindfleisch, T. C., J. A. Dunne, H. J. Frieden, W. D. Stromberg, and R. M. Ruiz, Digital processing of the Mariner 6 and 7 pictures, Jour. Geophys. Res., 76, 394, 1971.

Sagan, C., J. Veverka, P. Fox, R. Dubisch, J. Lederberg, E. Levinthal, L. Quam, R. Tucker, J. B. Pollack, and B. A. Smith, Variable features on Mars: preliminary Mariner 9 television results, Icarus, 17, 346, 1972.

Schultz, P. H., A preliminary morphologic study of the lunar surface, PhD. thesis, Univ. of Texas, Austin, 1972.

Sharp, R. P., L. A. Soderblom, B. C. Murray, and J. A. Cutts, The surface of Mars, 2, uncratered terrains, Jour. Geophys. Res., 76, 331, 1971.

Strom, R. G., Analysis of lunar lineaments. I. tectonic maps of the Moon, Lunar and Planetary Lab. Commun. 2, Tucson, Arizona, 205, 1964.

de Vaucouleurs, G., MM '71 Mars planning chart, Jet Propul. Lab., Pasadena, Calif., 1971.

Webb, C., Practical use of the fast fourier transform (FFT) algorithm in time series analysis, Univ. Texas Applied Res. Labs., ARL-TR-70-22, Austin, 1970.

Wilson, R. C., E. L. Harp, M. D. Picard, and S. H. Ward, Chaotic terrain of Mars: a tectonic interpretation from Mariner 6 imagery, Geol. Soc. America Bull., 84, 741, 1973.

Figure 1. Lineations mapped on the unrectified version of Mariner frame 6N09 (the regions of Aram and Margaritifer Sinus, lower left). Contours of discernibility indices reflect the change in the ability to recognize topographically expressed lineaments. An index of three indicates that for recognition, a linear feature must be three times as broad as a comparable feature in Mariner frame 6N21 (the region Deucalionis Regio). Easily recognized lineations (w3) are represented by solid lines, whereas poorly recognized lineations (w1) are represented by dotted lines. The symbols 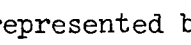 indicate negative relief, positive relief, and scarps, respectively. Such symbols attached to dotted lines represent marginally recognized lineations (w2).

FIGURE 1

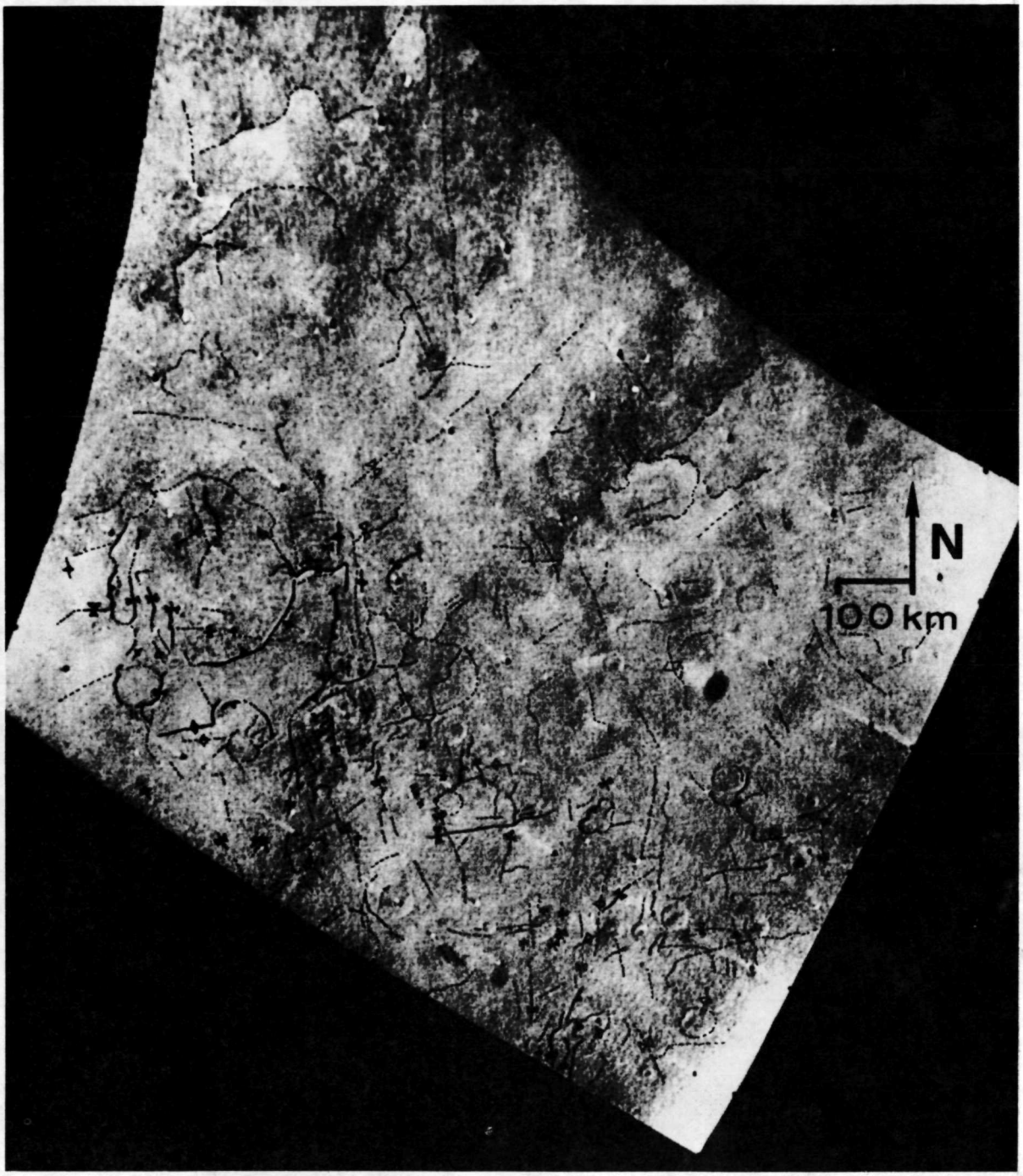

Figure 2. Lineations mapped on the rectified (orthographically projected) versions of Mariner frame 6N09. See Figure 1 for definition of symbols.

Figure 3. Rose diagrams of lineations from the unrectified version (Figure 3a) and orthographically projected version (Figure 3b) of Mariner frame 6N09. The upper half of each rose diagram uses the number of lineations, whereas the lower half illustrates lineations weighted by their length. Lineations (w3-w2) recognized as topographic features are to the right; lineations (w1) not recognized as topographic features are to the left. Arrows on the rose diagrams in Figure 3c note coherent noise trends on unprocessed photographs. Values within each rose diagram indicate the number of lineations used.

MARINER 6N09

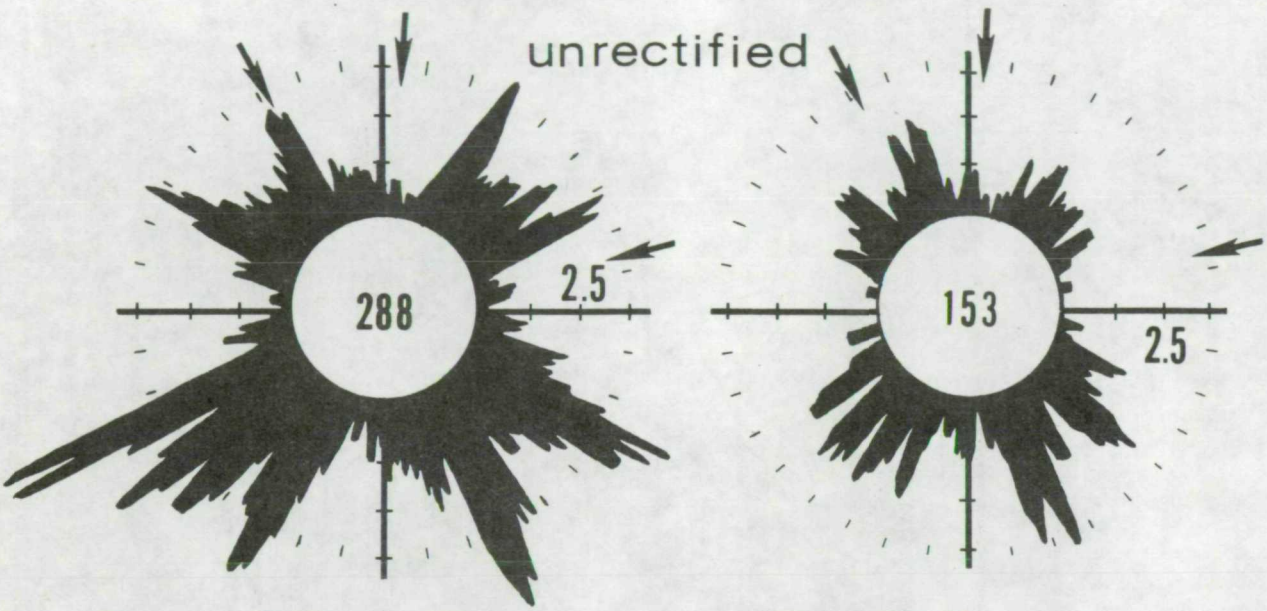

a. w1 lineations w3-w2 lineations

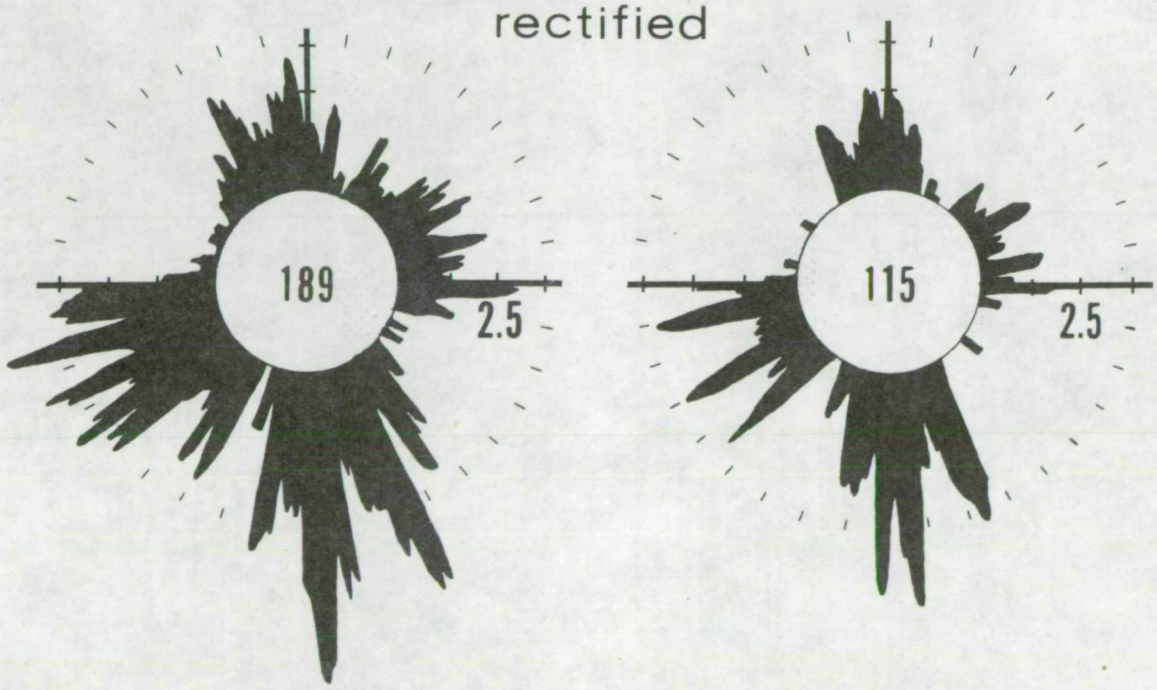

b. w1 lineations w3-w2 lineations

FIGURE 3

Figure 4. Rose diagrams for Mariner frames 6N13 and 6N21. The upper half of each rose diagram utilizes the number of lineations, whereas the lower half illustrates lineations weighted by their length. Lineations (w3-w2) recognized as topographic features are to the right; lineations (w1) not recognized as topographic features are to the left.

MARINER 6N13

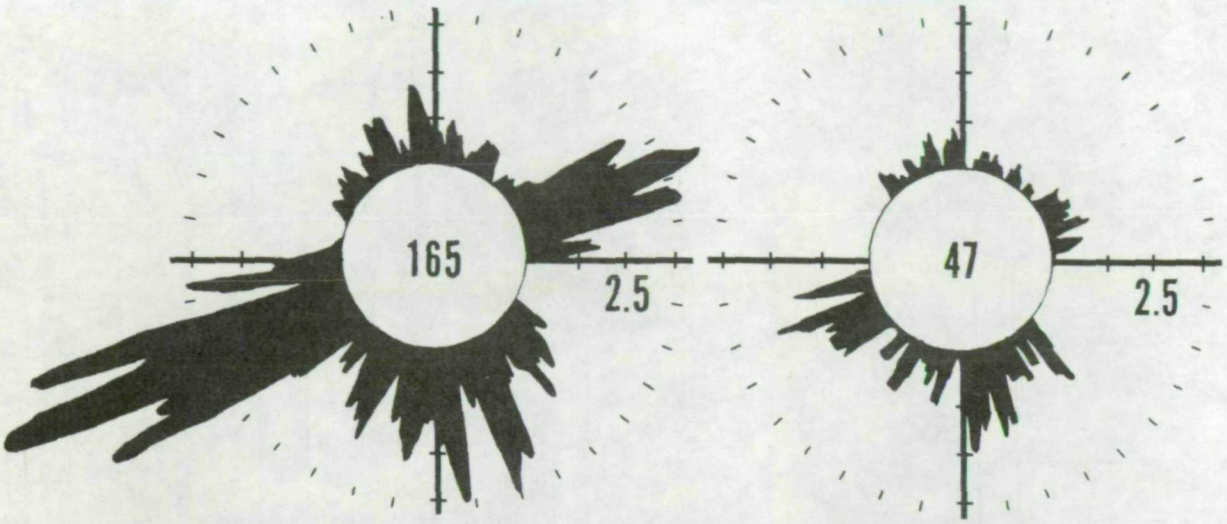

w1 lineations w3-w2 lineations

MARINER 6N21

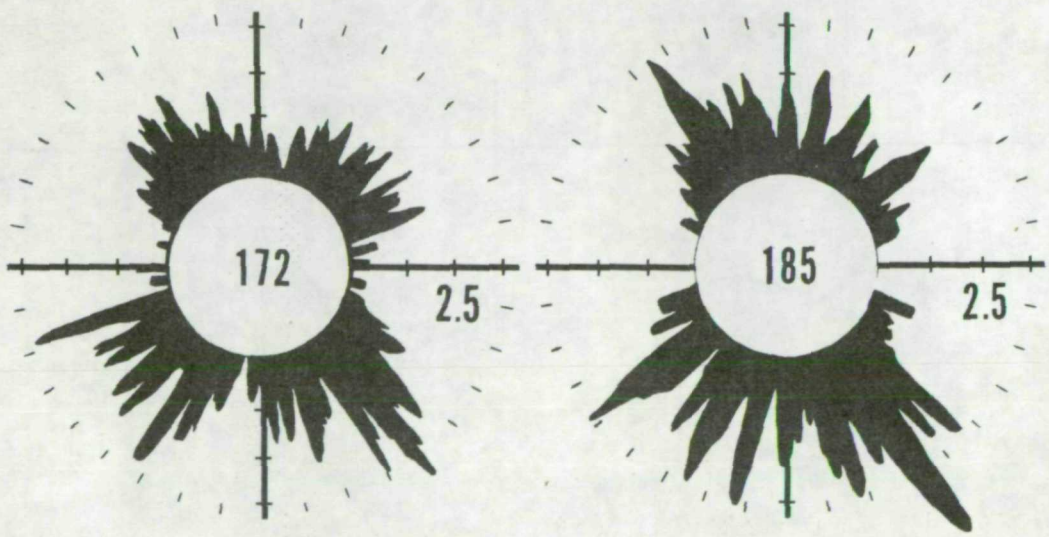

w1 lineations w3-w2 lineations

FIGURE 4

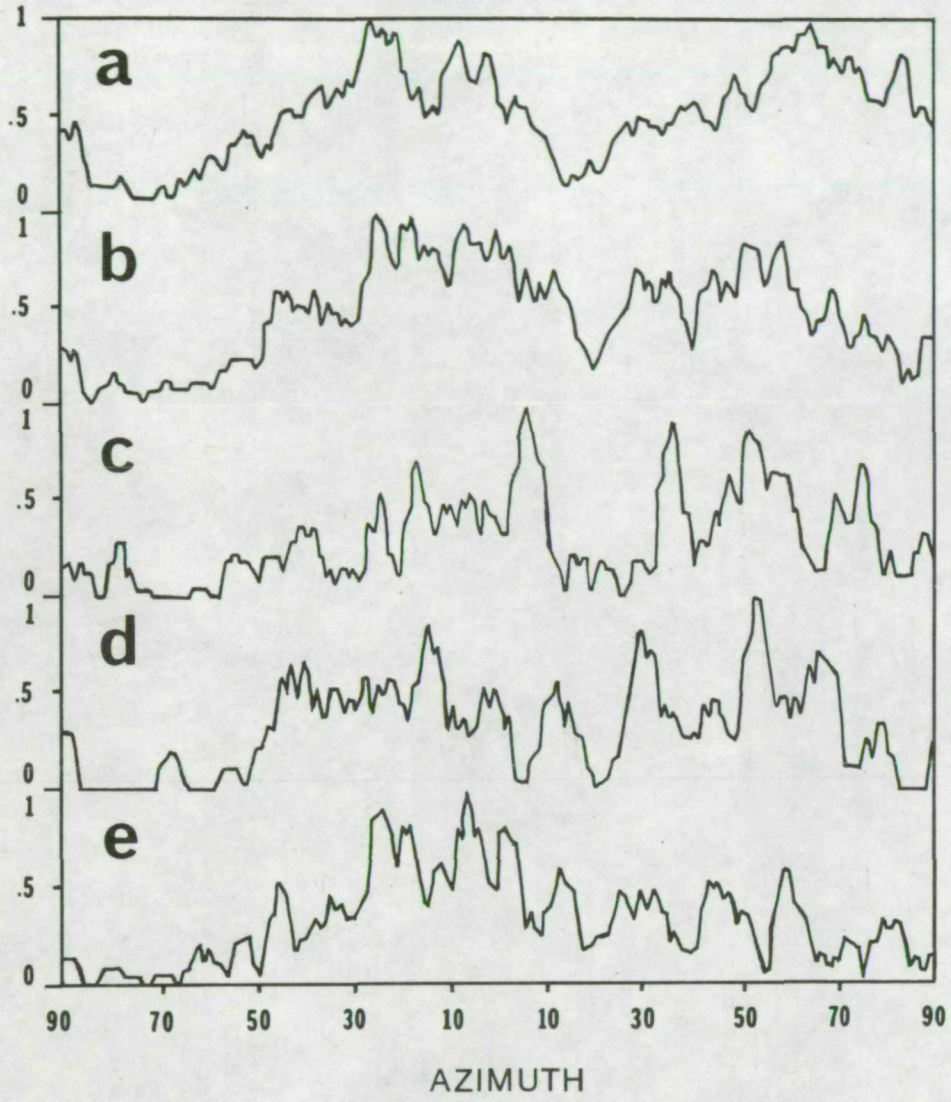

Figure 5. Frequency-azimuth distributions of 1506 least significant (w1) lineations (Figure 5a) and 775 most significant (w3-w2) lineations (Figure 5b) from rectified Mariner frames 6N09, 11, 13, 17, 19, 21 and 23. Figure 5c shows the distribution of 185 w3-w2 lineations from Margaritifer Sinus; Figure 5d, 219 w3-w2 lineations from Meridiani Sinus; and Figure 5e, 341 w3-w2 lineations from Deucalionis Regio. Lineations have been weighted by their length, and the distributions are normalized to the maximum peak in each data set.

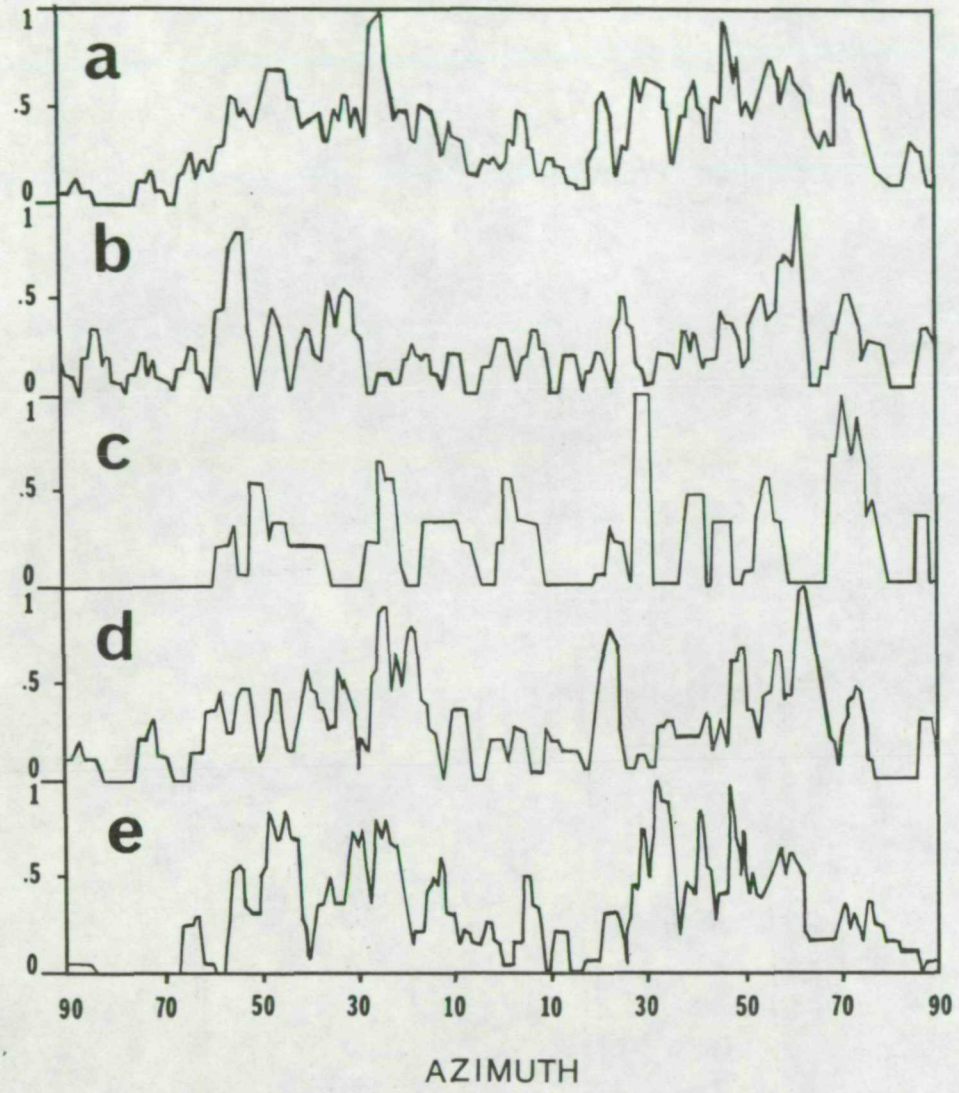

Figure 6. Frequency-azimuth distributions of 259 trends of crater walls (Figure 6a) and 121 crater chain alignments (Figure 6b) from rectified Mariner frames 6N09, 11, 13, 17, 19, 21, and 23. Figure 5c shows 35 trends of crater walls from Margaritifer Sinus; Figure 5d, 102 trends from Meridiani Sinus; and Figure 5c, 259 trends from Deucalionis Regio. Each crater-wall trend and crater chain alignment are weighted subjectively on a scale from 1 to 3. The distributions are normalized to the maximum peak in each data set.

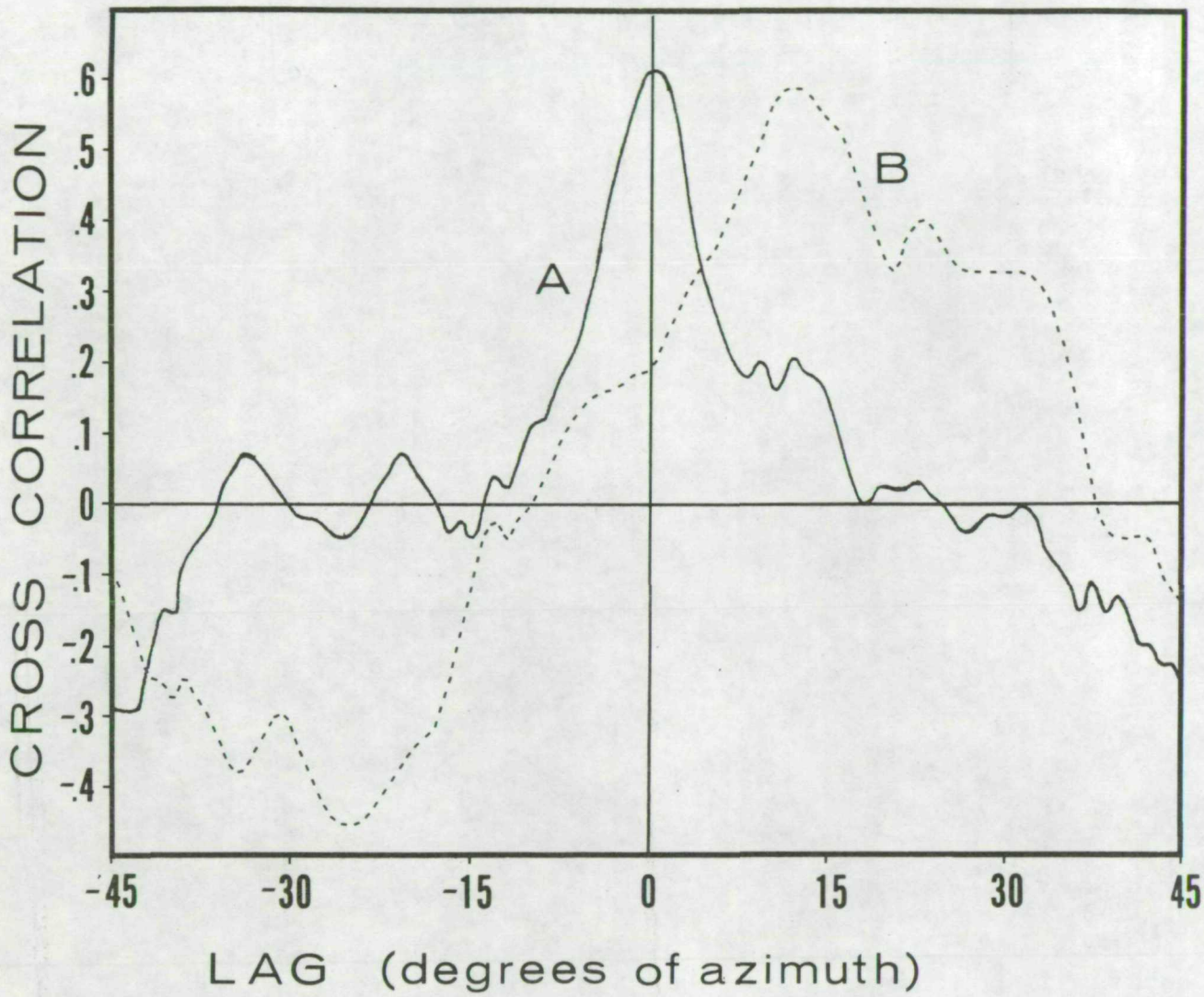

Figure 7. Cross correlations between frequency-azimuth distributions of w1 lineations from unrectified frames 6N09 and 6N17 (curve A); cross correlations between distributions of w1 lineations from corresponding orthographically projected frames (curve B).

Figure 8. Rose diagrams from photometrically defined regions for w3-w2 lineations, which are recognized as topographic features (top half of each rose diagram) and for w1 lineations, which are not recognized as topographic features (bottom half of each rose diagram). Data for Deucalionis Regio include the light area Aram, and Margaritifer Sinus includes the large canyon Eos. Values within rose diagrams indicate number of lineations used. Lineations are weighted statistically by length.

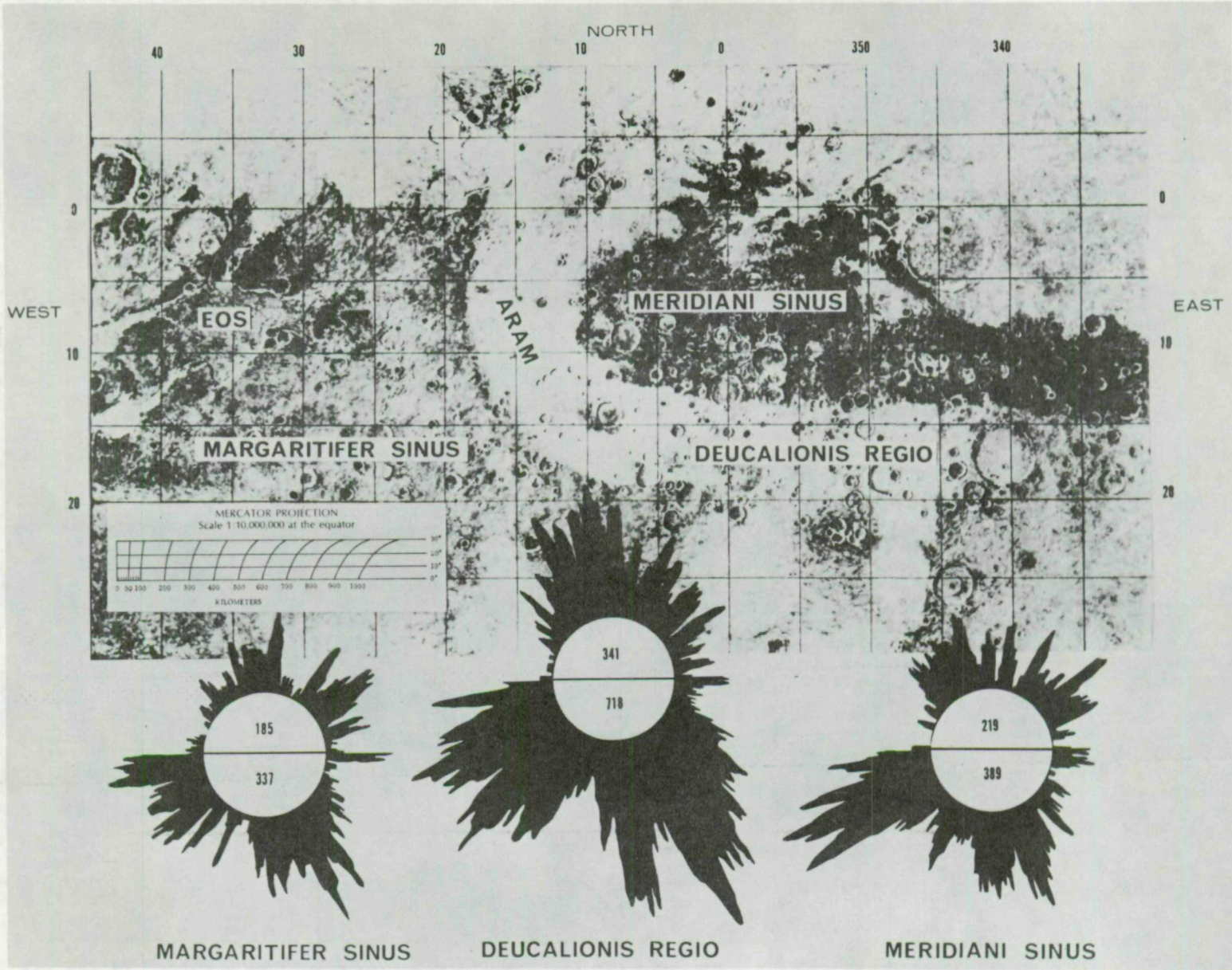
NORTH
40
30
20
10
0
350
340
0
10
20
WEST
EAST
EOS
ARAM
MERIDIANI SINUS
MARGARITIFER SINUS
DEUCALIONIS REGIO
MERCATOR PROJECTION
Scale 1:10,000,000 at the equator
KILOMETERS
185
337
341
718
219
389
MARGARITIFER SINUS
DEUCALIONIS REGIO
MERIDIANI SINUS

FIGURE 8

Figure 9. Lineations mapped on rectified frame 6N21. The approximate boundary between the lower albedo region, Meridiani Sinus (above) and the higher albedo region, Deucalionis Regio (below), is accompanied by numerous rillelike lineations. The albedo contrast between these regions is not obvious owing to the enhancement of small-scale contrast differences (maximum discriminability photographs). See Figure 1 for definition of symbols.

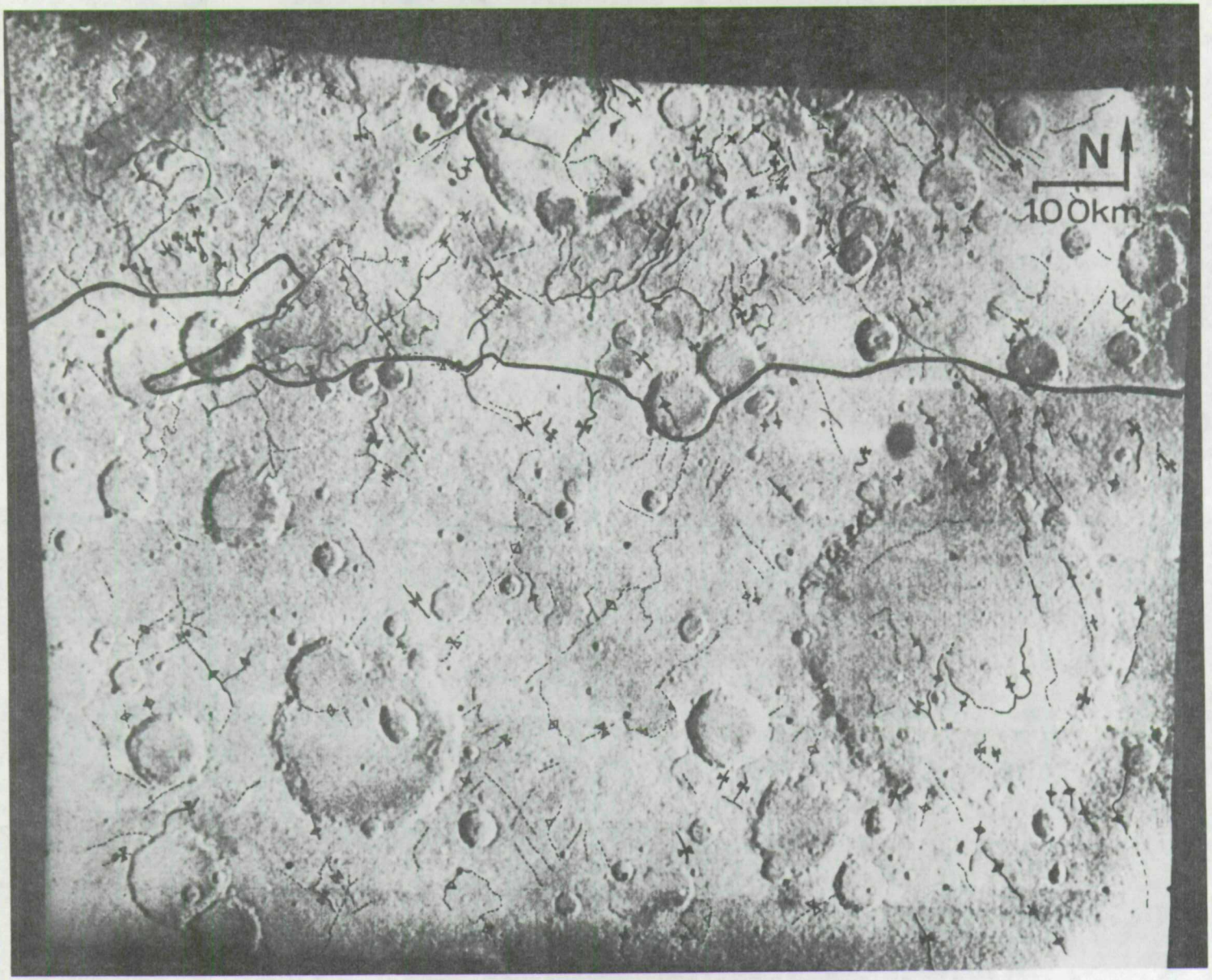

FIGURE 9